J Mater Sci: Mater Med (2015) 26:200
DOI 10.1007/s10856-015-5531-2



Original Research

# Oxygen diffusion in marine-derived tissue engineering scaffolds

**E. Boccardi[1] · I. V. Belova[2] · G. E. Murch[2] · A. R. Boccaccini[1] · T. Fiedler[2]**

Received: 1 June 2015 / Accepted: 19 June 2015 / Published online: 26 June 2015


**Abstract** This paper addresses the computation of the effective diffusivity in new bioactive glass (BG) based tissue engineering scaffolds. High diffusivities facilitate the supply of oxygen and nutrients to grown tissue as well as the rapid disposal of toxic waste products. The present study addresses required novel types of bone tissue engineering BG scaffolds that are derived from natural marine sponges. Using the foam replication method, the scaffold geometry is defined by the porous structure of *Spongia Agaricina* and *Spongia Lamella*. These sponges present the advantage of attaining scaffolds with higher mechanical properties (2–4 MPa) due to a decrease in porosity (68–76 %). The effective diffusivities of these structures are compared with that of conventional scaffolds based on polyurethane (PU) foam templates, characterised by high porosity (>90 %) and lower mechanical properties (>0.05 MPa). Both the spatial and directional variations of diffusivity are investigated. Furthermore, the effect of scaffold decomposition due to immersion in simulated body fluid (SBF) on the diffusivity is addressed. Scaffolds based on natural marine sponges are characterised by lower oxygen diffusivity due to their lower porosity compared with the PU replica foams, which should enable the best oxygen supply to newly formed bone according the numerical results. The oxygen diffusivity of these new BG scaffolds increases over time as a consequence of the degradation in SBF.

✉ T. Fiedler
thomas.fiedler@newcastle.edu.au

[1] Department of Materials Science and Engineering, Institute of Biomaterials, University of Erlangen-Nuremberg, 91058 Erlangen, Germany

[2] School of Engineering, University of Newcastle, Callaghan, NSW 2287, Australia

## 1 Introduction

Bone is characterized by a high regenerative capability, which means that the majority of fractures will heal without the need for surgical intervention. Despite this, large bone defects usually lack the template for an orchestrated regeneration and require surgery [1]. The present 'gold standard' is to harvest 'donor' bone from a non-load-bearing site and transplant it into the defect site of the same patient [1, 2]. The main limitations of autografts are the additional operating time, healing of both donor and implant sites, as well the pain and the increased risk of infections [2, 3]. An alternative strategy is tissue engineering, which involves the application of the principles and methods of engineering and life sciences in order to develop biological substitutes that restore, maintain or improve tissue function [4]. One of the most investigated fields of tissue engineering is the use of porous 3-D engineered scaffolds to induce bone regeneration. The idea is to reproduce the bone tissue's morphology using bioactive materials, which have the capability to integrate with the biological environment and to promote the regeneration of natural tissue [5, 6]. The challenge is the design of materials able to match not only the biological but also the mechanical properties of real bone tissue [4]. Since its discovery by Hench in 1969, Bioglass® 45S5, is still one of the most important biomaterials for bone defect repair [7]. This bioactive glass (BG), once in contact with the biological fluids, is able to form a bond with both soft and hard tissue. Moreover, the formation of a layer of carbonated hydroxyapatite (HCA) at the surface of the material occurs, which is similar to the mineral phase of bone. In addition, the release of soluble silica and calcium ions from BG is able to stimulate the gene expression of osteoblasts and induce angiogenesis in vitro and in vivo [7–9]. Bioglass®

has been used in several clinical applications in bulk-form and as a particulate in non-load bearing sites for bone grafting and for the prevention of dental hypersensitivity [8]. So far, porous 3-D Bioglass®-based scaffolds are not yet available for clinical applications although several techniques have been developed for their production, starting with the foam replica method introduced in 2006 [10]. The main challenge is the fabrication of a scaffold which has at the same time high porosity and sufficient mechanical stability as natural bone. In recent times, efforts have focused on the production of porous Bioglass®-based scaffolds with increased mechanical properties due to a reduction of the total porosity without affecting the interconnectivity of pores. Cunningham et al. proposed the use of natural marine sponges as a sacrificial template for the production of porous hydroxyapatite-based scaffolds via a replica technique instead of the polyurethane (PU) foam [11]. However the use of natural marine sponges has not been considered so far for the production of BG scaffolds.

The diffusivity in tissue engineering scaffolds is important for the supply of new tissue with oxygen and nutrients as well as the removal of toxic waste products. Previous research mainly addressed the diffusion of oxygen within tissue engineering scaffolds. A comprehensive study [12] investigated oxygen diffusion in polycaprolactone scaffolds and showed a strong relationship between scaffold porosity, tortuosity and diffusivity. Scaffold resorption and the formation of tissue changes the scaffold diffusivity and can be considered by introducing a time-dependent diffusivity [13]. Analogous to a previous work on scaffold diffusivity [14] the present study focuses on the late stage of tissue regeneration where the scaffold porosity is completely occupied by regrown tissue but prior to vascularization. This can be considered a worst case scenario since subsequent vascularization will significantly improve the oxygen supply of tissue. The previous study [14] investigated the diffusivity in replicated PU foam scaffolds, sol–gel cast scaffolds and robocast scaffolds. The present study extends this work by addressing Bioglass®-based scaffolds prepared using the natural marine sponges *Spongia Agaricina* (SA) and *Spongia Lamella* (SL) as sacrificial templates (see Fig. 1). Furthermore, for the first time, the effect of partial scaffold resorption on the diffusivity is considered.

## 2 Materials and methods

### 2.1 Scaffolds fabrication and characterisation

The starting material in the manufacturing of the replicated scaffolds was melt-derived 45S5 Bioglass® powder (particle size 5 μm). The sacrificial templates for the scaffold production were: PU packaging foams (45 ppi) purchased from Eurofoam Deutschland GmbH Schaumstoffe, marine sponges SA and SL harvested respectively from the Indo-Pacific Ocean (Pure Sponges, UK) and Mediterranean Sea (Hygan Products Limites, UK) and belonging to the "Elephant Ear" family. Harvesting of all natural sponges was performed in an environmentally-friendly manner, as specified by the supplier companies. These marine sponges (see Fig. 1), thanks to the millenarian evolution for water filtration, are promising precursors for the production of bone tissue engineering scaffolds due to their interconnected porous architecture [15]. The use of these sponges presents several advantages, including the possibility of attaining higher mechanical properties than those of scaffolds made by the foam replica method (up to 4 MPa) due to a decrease in porosity (68–76 %) without affecting the pores interconnectivity (higher than 99 %) [18]. The pore structure obtained possesses not only pores with a diameter in the range 150–500 μm, necessary to induce bone ingrowth, but also pores in the range of 0–200 μm which are requested for complete integration of the scaffold and for neovascularization [16, 17]. In this way, it is possible to combine the main properties that a three-dimensional scaffold should have for bone regeneration: interconnected and high porosity, adequate mechanical properties and bioactivity.

The investigated 45S5 Bioglass® scaffolds were produced by the replica technique, as reported by Chen et al. [10]. The details of the scaffolds fabrication are presented elsewhere [18]. Briefly the slurry was prepared by dissolving polyvinyl alcohol (PVA) in deionized water at 80 °C (ratio 0.01 mol $L^{-1}$). The 45S5 Bioglass® powder was then added to 25 mL PVA-water solution with a concentration of 40 wt%. The sacrificial templates were immersed into the slurry for 10 min. The foams were retrieved from the suspension and the extra slurry was completely squeezed out. The samples were dried at room temperature and the dip-coating procedure was repeated two or three times. After the second and third coating, the superfluous slurry was completely removed using compressed air. The PU foams and SL were immersed in the Bioglass® slurry three times, while SA only required two coats. The post-foaming heat treatment for the burn-out of the sacrificial template and sintering of the 45S5 Bioglass® was: 400 °C/1 h and 1050 °C/1 h, respectively. The heating and the cooling down rates used were 2 and 5 °C $min^{-1}$, respectively. The density of the foams, $\rho_F$, was measured using the mass and dimensions of the sintered cylinders. The porosity, $\Phi$, was calculated using the formula:

$$\Phi = (1 - \rho_F/\rho_{45S5}) \quad (1)$$

where $\rho_{45S5} = 2.7$ g $cm^{-3}$ (the theoretical density of 45S5 Bioglass® not considering change of density due to

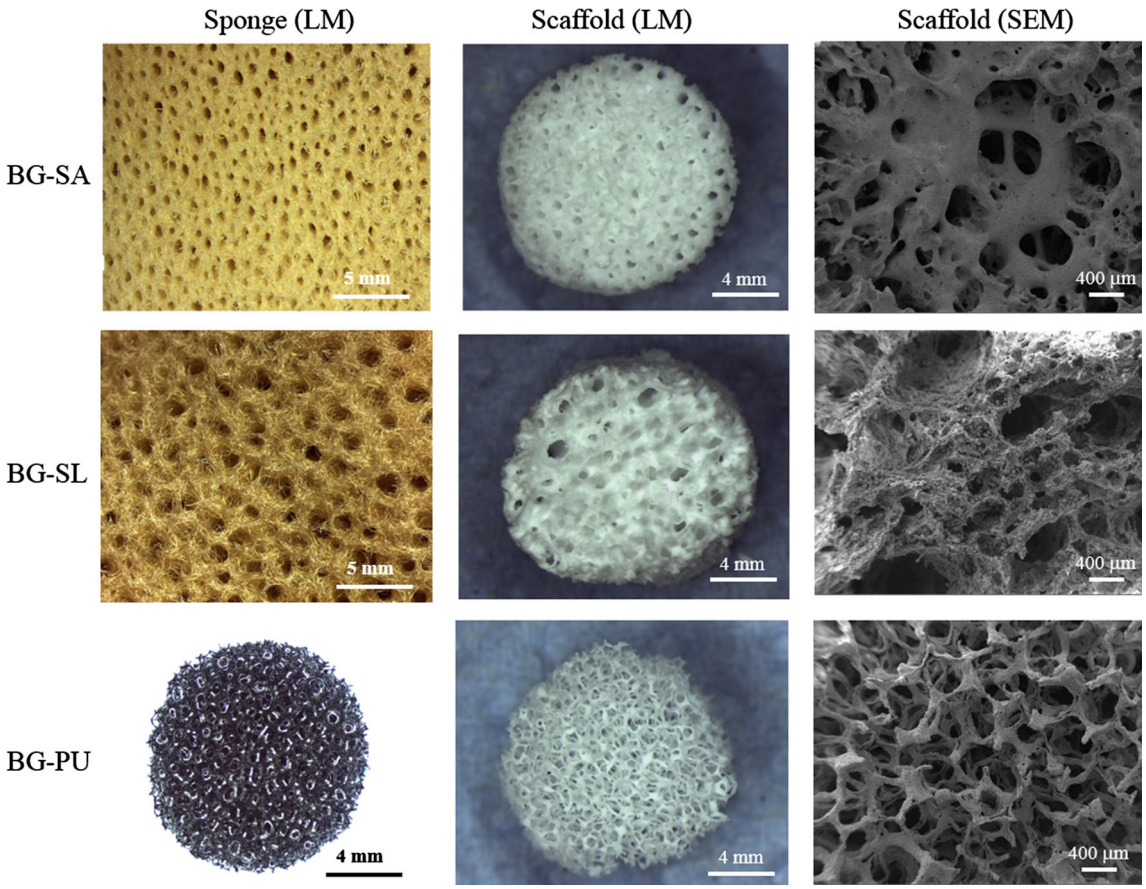


**Fig. 1** Replicated scaffolds derived from *Spongia Agaricina* (BG-SA), *Spongia Lamella* (BG-SL) and polyurethane foam (BG-PU): light microscopy (LM) and scanning electron microscopy (SEM)

crystallisation) [19]. It should be mentioned that this porosity value includes micro-porosity within the scaffold struts that is introduced by the pyrolysis of the organic material and subsequent sintering (see the SEM images Fig. 1).

To characterise scaffolds bioactivity cylindrical Bioglass®-based scaffolds were immersed in simulated body fluid (SBF) with a 1.5 g $L^{-1}$ ratio for 28 days [20]. The solution was kept in a plastic container at 37 °C in a shaking incubator (90 rpm). The solution was renewed every 48 h in order to better mimic in vitro the in vivo interaction between BG porous scaffolds and biological fluid. At the end the foams were collected, rinsed with millipore water, frozen overnight and freeze dried for at least 2 h.

The structure of the original and partially resorbed foams was observed using a micro-computed tomography system, micro-CT (Skyscan 1147 Micro-CT) and scanning electron microscopy (SEM) (AURIGA 0750 Zeiss). The pore size distribution was characterised on 2D sections extracted from micro-CT reconstructions using ImageJ analysis software. A constant voxel side length of 6.5 µm was used in all scans to obtain accurate representations of the complex scaffold geometry. Samples were aligned so that the *x*-direction of the scans coincides with the pore orientation of SL and SA. Scans were obtained from scaffolds directly after manufacturing (original) and from partially resorbed scaffolds that were immersed in SBF for 28 days (resorbed). Different samples had to be used for the scans of original and resorbed scaffolds since otherwise the electron beam of the tomography could have altered the structure of the scaffold material and thus distorted the results. In order to eliminate calculation errors due to uneven sample surfaces cubical sub-volumes were extracted from the center of each $\mu$CT data set. Figure 2 shows the spatial porosity variation within these cubes in the perpendicular *x*-, *y*- and *z*-directions.

The porosity of *BG-SA* (i.e. scaffolds derived from *Spongia Agaricina*) shows a fluctuation around an average value of 68.2 % (original, full lines) and 72.3 % (resorbed, dashed lines). In contrast, *BG-SL* (SL) exhibits a systematic decrease of porosity in the pore (*x*-) direction from 81.6 to 51.8 %. This deviation is caused by the differing geometries of inhalant and exhalant surfaces of the marine animal

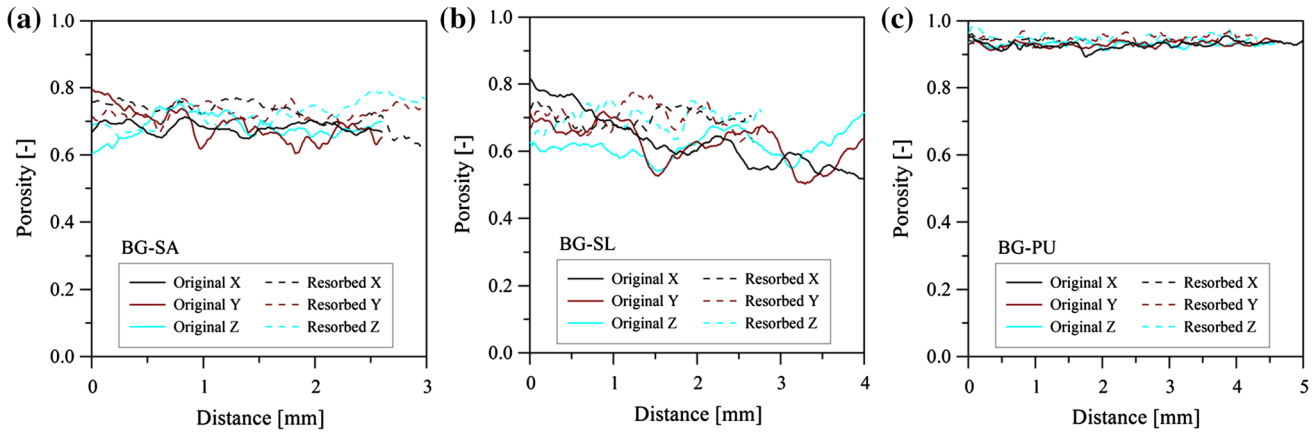


**Fig. 2** Porosity variation in scaffolds: **a** BG-SA, **b** BG-SL, **c** BG-PU

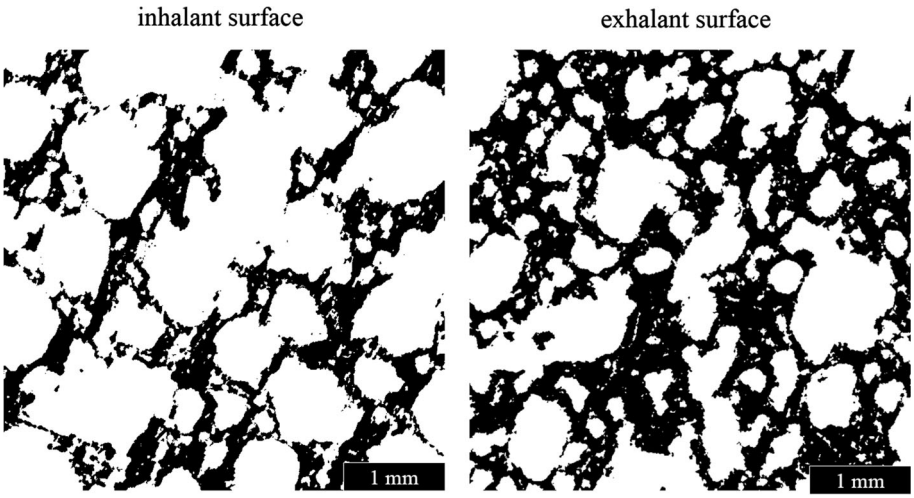


**Fig. 3** Micro computed tomography images of the original BG-SL scaffold

shown in Fig. 3. For the orthogonal *y*- and *z*-directions the porosity values oscillate around the average values of 61.2 % (original) and 69.8 % (resorbed). The scanned *BG-SL* scaffold (resorbed) was significantly smaller and thus does not exhibit the distinct density change between inhalant and exhalant surfaces. The analysis of the *BG-PU* (PU foam) samples reveals an almost constant porosity with an average value of 93.5 % (original) and 94.7 % (resorbed) porosity.

## 2.2 Lattice Monte Carlo method

The effective oxygen diffusivity in tissue engineering scaffolds was determined using the Lattice Monte Carlo method [21, 22]. This numerical method simulates random walks of probing particles within lattice models that represent the target geometry, in this case the interconnected porosity of tissue engineering scaffolds. For geometric accuracy, lattice models are derived directly from the high resolution micro-computed tomography scans. The computed particle mobility is evaluated to determine the effective diffusivity. The method has been successfully applied towards the determination of effective oxygen diffusivity in scaffolds [14], thermal diffusivity [23], and mass diffusivity [22]. Detailed descriptions of the method can be found in the literature [21, 24].

Following a previous study on diffusivity in scaffolds [14], the interconnected pores (porosity $\Phi$) are assumed to be completely occupied by regenerated tissue with a bulk diffusivity $D_T$. At the same time, vascularization is assumed to be incomplete and not yet contributing to the oxygen transport. The diffusivity of the scaffold material itself is approximated by zero. Thus, the scaffold material acts as a local diffusion barrier and reduces the effective diffusivity $D_{eff}$ of the embedded tissue. The dimensionless diffusivity $D^*$ is calculated as $D_{eff}/D_T$ and allows the extrapolation of results to various types of tissue. This modelling approach assumes a worst case scenario (i.e. no vascularization and no

diffusion in the scaffold material) and hence determines the important lower bound for diffusivity.

### 2.3 Analytical expressions

Depending on the geometry of the phase distribution in a composite material there are a number of theoretical approaches available for the evaluation of their effective properties [25]. Since the geometry of the *BG-PU* scaffold structure is essentially different from the *BG-SA* and *BG-SL* scaffold structures a different theoretical approach for a description of the *BG-PU* effective diffusivity is required.

#### 2.3.1 BG-SA and BG-SL scaffold structures

Due to the bimodal nature of the pore sizes distribution for *BG-SA* and *BG-SL* scaffold structures the most suitable approach for these materials was considered as follows. We consider the matrix phase that consists of the Bioglass® with smaller sized interconnecting pores (i.e. micro-porosity), and the large pores as the inclusions into the matrix phase. Next, we assume that the amount of porosity in the matrix phase is a fraction $g$ of the total porosity $\Phi$. Then the total volume fraction $\Phi_m$ of the matrix phase is

$$\Phi_m = 1 - \Phi + g\Phi \tag{2}$$

and the normalized effective diffusivity $D_m$ of the matrix phase is

$$D_m = g\Phi/(1 - \Phi + g\Phi). \tag{3}$$

For the total normalized effective diffusion coefficient there is a Maxwell-type [23, 26] expression available:

$$D_M^{eff} = D_m\left(1 - \frac{3(D_m - 1)(1 - \Phi_m)}{2D_m + 1 + (D_m - 1)(1 - \Phi_m)}\right) = \frac{g\Phi(1 + 2\Phi)}{1 - 2\Phi + g\Phi(4 - \Phi) + \Phi^2}. \tag{4}$$

The fraction $g$ is not known and we will treat $g$ as a fitting parameter using results of Lattice Monte Carlo simulations of the effective normalized diffusion coefficient.

#### 2.3.2 BG-PU scaffold structure

The BG-PU scaffold structure is clearly a high-porosity open cell structure (see Figs. 1, 2). It was found [23] that for this type of structure the Dulnev model [27] provides the best result. We assume here that the model should describe well both diffusion along the struts [22] and diffusion in the open space of the structure (with necessary adjustments). Then, according to this model, the effective normalized diffusion coefficient is simply expressed as:

$$D_D^{eff} = \left(1 - (1 - \Phi)^{2/3}\right). \tag{5}$$

The generalized Scaling relation approach [20]:

$$D^{eff} = \Phi^n \tag{6}$$

will be used for comparison as well. In [14] it was found that Eq. (6) gives the best agreement for the usual scaffolds structures when $n \approx 2$.

## 3 Results and discussion

In the following, results for the oxygen diffusion simulation of two newly developed Bioglass®-based scaffolds, BG-SA and BG-SL, are presented. Moreover a comparison with the conventional scaffolds based on PU foam template is given. BG-SA and BG-PU are characterised by almost constant porosity values along the ($x$-) direction. After immersion in SBF, BG-SA shows an increase in total porosity, while BG-PU scaffold does not exhibit any significant change between the original and the incubated samples. In contrast, BG-SL exhibits a significant difference in pore dimension in the ($x$-) direction due to the differing geometries of inhalant and exhalant surfaces. Figure 4 shows the dimensionless diffusivity plotted versus scaffold porosity. As previously discussed, the simulation model assumes that the newly regenerated tissue has completely occupied the interconnected pores. Absolute diffusivities (not shown) for a particular tissue type are obtained simply by multiplication by the corresponding bulk tissue diffusivity $D_T$. For comparison, dimensionless diffusivities of the present study are shown along with data from a previous study [14]. All markers are average values and bars represent anisotropic minima and maxima. In addition to the simulation results the parabolic function $D = \Phi^2$ (Eq. 6) is plotted as a solid line.

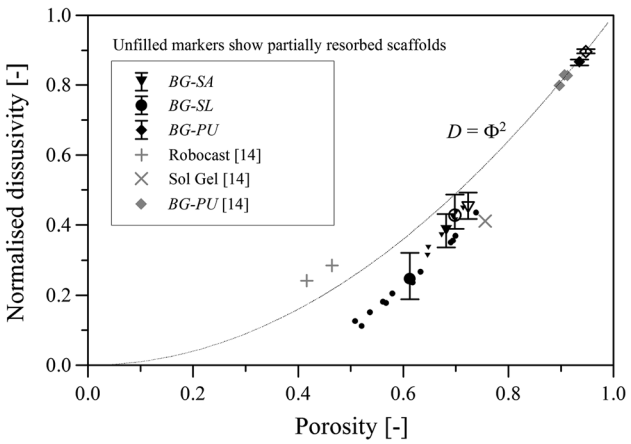


**Fig. 4** Normalised diffusivity plotted versus scaffold porosity

Diffusivities in *BG-PU* scaffolds are represented by diamond markers. Good agreement with the results of a previous study [14] is observed. Partial scaffold resorption (unfilled diamond marker) due to 28 days immersion in SBF increases both the *BG-PU* scaffold porosity and diffusivity. The diffusion in *BG-PU* scaffolds is well described by the parabolic function Eq. (6). In contrast, the dimensionless diffusivities in natural marine-derived scaffolds *BG-SL* and *BG-SA* fall short of the $\Phi^2$ function. In addition, a distinct anisotropy is observed that will be further discussed below. Due to the strong porosity variation (see Fig. 2b) and in order to investigate the variation of diffusivity in the scaffolds the geometry of original *BG-SL* and *BG-SA* was subdivided into non-intersecting prisms and diffusivities determined for each sub-volume. The results are indicated by the small filled circular and triangular markers and the large marker shows the average value. The distinct variation of diffusivity observed for the sub-volumes is attributed to changes in porosity and to a lesser degree to random structural variations of the biological template (marine sponges). Scaffolds of the same type (i.e. either *BG-SA* or *BG-SL*) and a similar porosity also exhibit comparable diffusivities indicating that diffusivity is governed by porosity. The data also shows that *BG-SA* scaffolds exhibit a higher diffusivity than *BG-SL* at the same porosity. The partially resorbed *BG-SL* (unfilled circle) exhibits a significantly higher porosity and diffusivity that is similar to the two data points of *BG-SA*. It is interesting to note that the *maximum* directional diffusivity in the marine-derived scaffolds is in close vicinity to the $\Phi^2$ function.

Results of the two analytical expressions (4) and (5) are presented in Fig. 5. In addition, the dimensionless diffusivities obtained by means of LMC are shown by symbols: filled circles were used for the marine-derived scaffolds (*BG-SA* and *BG-SL*) and filled diamonds for the PU foam-based scaffolds (*BG-PU*). The solid line represents the Maxwell-type expression Eq. (4) that was used for diffusion modelling of the *BG-SA* and *BG-SL* scaffolds structures. The parameter $g$ was varied to get the best fit to the computer simulated data. It was found that the micro-porosity fraction $g \approx 0.036$ (or 3.6 %) gives the best agreement with results of numerical simulations. This value of micro-porosity $g$ is reasonable, given that the total pore interconnectivity of these scaffold structures was found to be higher than 99 %. Diffusivities for both original and resorbed samples follow the proposed model very well. The dashed line represents the result of the Dulnev expression, Eq. (5), which was suggested to model the diffusion behavior of the *BG-PU* scaffold structure. Comparison with Fig. 4 shows that the $\Phi^2$ function gives rather better agreement for this scaffold type.

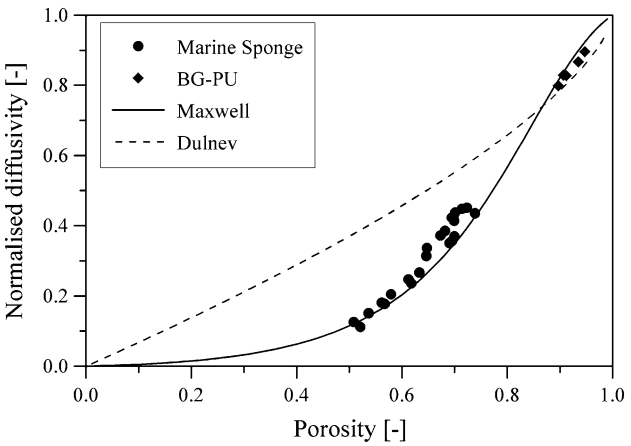


**Fig. 5** Analytical models for the effective diffusivity of tissue engineering scaffolds

Table 1 aims to correlate the effective diffusivity $D_{\text{eff}}$ and structural parameters of tissue engineering scaffolds. To this end, the mean scaffold strut thickness $t$ and the mean pore size $s$ were determined using the ImageJ plugin BoneJ [28]. Furthermore, the coefficients of variation ($CV_{t,s}$) for scaffold thickness and pore size were calculated. As expected, the scaffold thickness $t$ generally decreases and the pores size $s$ increases due to immersion in SBF. The apparently contradicting decrease of the average pore size for resorbed SL (*BG-SL*) is attributed to the use of a different sample for the resorption study. The resorbed *BG-SL* sample contains a predominantly exhalant surface structure. This surface has a smaller pore size (see Fig. 3) explaining the deviating value in the Table 1. It has been observed previously that the diffusivity is affected by the coefficient of variation $CV_s$ of the pore size [14]. A low value of $CV_s$ indicates uniform pore size resulting in a high diffusivity close to $\Phi^2$ (see Fig. 4). As an example, *BG-PU* scaffolds have low $CV_s$ and their data points coincide with the parabolic function. In contrast, the inhomogeneous structure of *BG-SL* causes high values of $CV_s$ and the dimensionless diffusivity falls short of the parabolic function. Furthermore, the high values of $CV_s$ are consistent with the bimodal nature of the pore size distribution in these scaffolds. Table 1 further shows the standard deviations of the diffusivities for the original scaffolds. A close correlation between the variation of pore size $CV_s$ and the standard deviation of diffusivity is found, i.e. a constant pore size yields a low variation of diffusivity.

Figure 6 shows anisotropy plots of diffusion in scaffolds. The graphs indicate directional diffusivities in the perpendicular *xy*, *xz* and *yz*-planes. In these plots, isotropic behavior is indicated by circular graphs as obtained for *BG-PU* (see. Fig. 6c). The degree of anisotropy can be quantified using the ratio $\chi$ between minimum and maximum diffusivity where a maximum possible value of unity

**Table 1** Diffusivities and structural parameters of tissue engineering scaffolds

| Structure | $D^*$ (–) | STDEV $D^*$ | $\Phi$ (%) | $t$ (μm) | $CV_t$ (–) | $s$ (μm) | $CV_s$ (–) |
|---|---|---|---|---|---|---|---|
| *BG-SA* (original) | 0.39 | 0.052 | 68.2 | 80 | 0.36 | 209 | 0.55 |
| *BG-SA* (resorbed) | 0.45 | – | 72.3 | 81 | 0.40 | 244 | 0.51 |
| *BG-SL* (original) | 0.25 | 0.107 | 61.2 | 103 | 0.55 | 335 | 0.74 |
| *BG-SL* (resorbed) | 0.43 | – | 69.8 | 86 | 0.38 | 268 | 0.64 |
| *BG-PU* (original) | 0.87 | 0.017 | 93.5 | 86 | 0.36 | 687 | 0.17 |
| *BG-PU* (resorbed) | 0.90 | – | 94.7 | 75 | 0.45 | 729 | 0.20 |

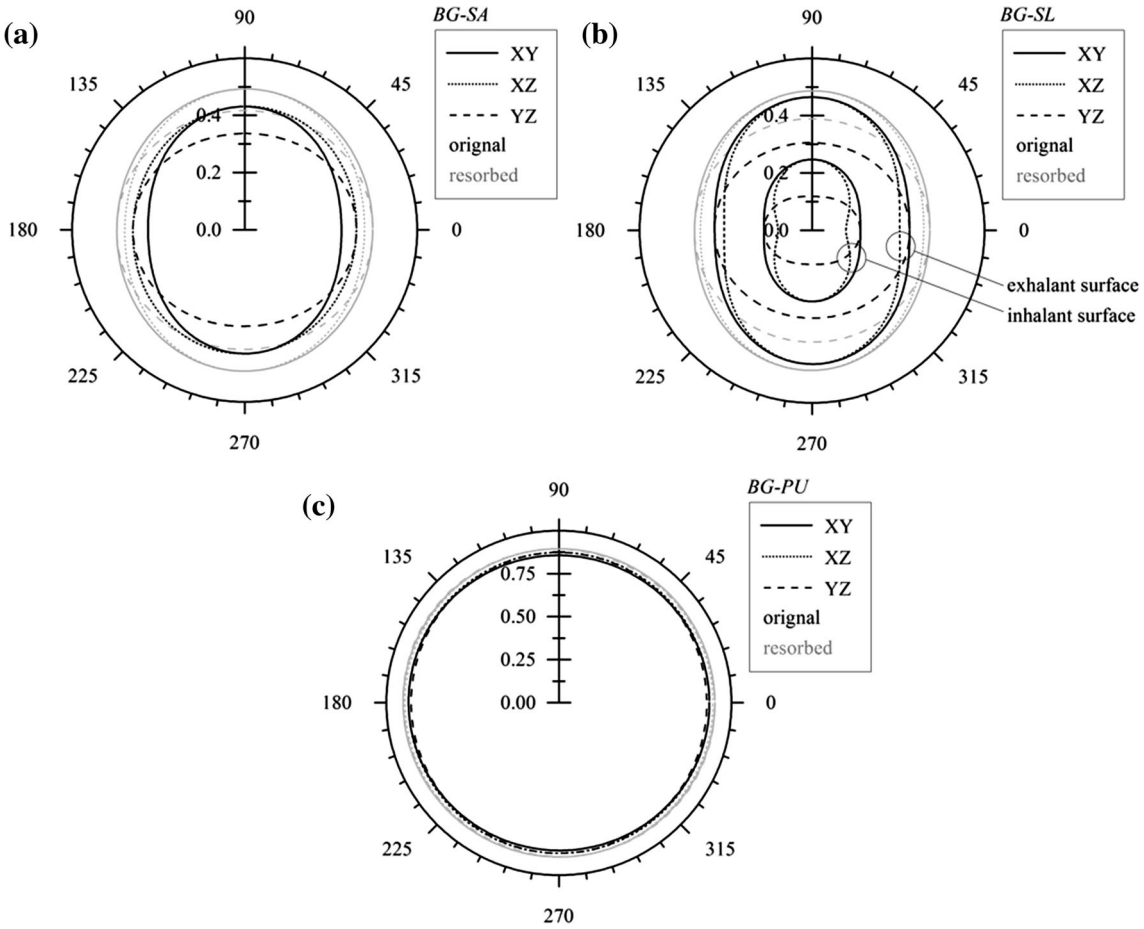


**Fig. 6** Anisotropy of normalized scaffold diffusivity

corresponds to perfect isotropy. In all plots, black lines show the results of original scaffolds whereas grey lines represent partially resorbed structures. As already observed in Fig. 4 higher values are found for the resorbed scaffolds.

In the case of *BG-PU* (see Fig. 6c) the ratio is $\chi = 0.98$ for both the original and the partially resorbed scaffold thus indicating isotropic diffusion properties. *BG-SA* is shown in Fig. 6a and moderate anisotropy is found. The corresponding anisotropy ratio is $\chi = 0.78$ (original) and $\chi = 0.85$ (resorbed) indicating that anisotropy decreases due to resorption. As expected, maximum values are found for the $x$-direction which is the predominant pore direction of SA. *BG-SL* shows a similar behavior; however, anisotropy is significantly stronger. Two datasets for original scaffolds are shown that represent the inhalant and exhalant surfaces, respectively. The maximum anisotropy ($\chi = 0.48$) is observed within the original exhalant surface. This can be explained by a large number of narrow channels formed by the tubular pores (see Fig. 3). Anisotropy is decreased in the inhalant area region ($\chi = 0.66$) and for the partially resorbed *BG-SL* scaffold ($\chi = 0.80$).

The present work aimed to describe only the architecture and the oxygen diffusivity in BG scaffolds based on natural marine sponges as a foam template. However, the challenge is the design of multi-functional scaffolds able to match at the same time not only the biological but also the mechanical properties of the real tissue and to support neovascularization. BG-PU scaffolds, thanks to their high porosity, exhibit the maximum oxygen diffusivity however, at the same time, their mechanical strength is limited. BG-SA and BG-SL scaffolds present lower oxygen diffusivity due to their structure porosity and tortuosity. The oxygen diffusivity of the natural marine sponges based scaffolds increases over time due to the degradation of the material after one month in SBF. This is an important result, as these structures are expected to dissolve once in the body and, ideally, at the same rate as the formation of the new tissue.

## 4 Conclusions

This paper investigated effective diffusivities in foam replicated tissue engineering scaffolds. The focus was scaffolds derived from the marine sponges SA and SL. Tissue engineering scaffolds act as diffusion barriers that decrease the intrinsic diffusivity of growing tissue. The results indicate a decrease to 39 % (*BG-SA*) and 25 % (*BG-LA*) of the corresponding bulk tissue diffusivity. Furthermore, the effect of scaffold resorption due to immersion in SBF for 28 days was addressed. The resulting increase in porosity caused increased effective diffusivities equal to 45 % (*BG-SA*) and 43 % (*BG-LA*) of the intrinsic value. A Maxwell-type analytical approach that successfully utilized the bimodal nature of the pore size distribution was proposed and investigated for diffusion modelling of these scaffold structures. It was found that a single fitting parameter $g$ (i.e. the micro-porosity) should be about 0.036 for good agreement with the diffusivities obtained numerically for both structures and for both original and resorbed stages. In addition, the anisotropy of the diffusivity was investigated. The degree of anisotropy was quantified by calculating the ratio $\chi$ of minimum and maximum directional diffusivities. Strong anisotropy was found for *BG-LA* ($\chi \geq 0.48$) and moderate anisotropy for *BG-SA* ($\chi \geq 0.78$). This directional variation of diffusivity can be explained by the tubular geometry of pores in the marine sponges. In contrast, scaffolds replicated from PU showed isotropic diffusion behavior ($\chi \geq 0.98$). In comparison to scaffolds manufactured using sacrificial PU foam templates (*BG-PU*) a distinct decrease of the diffusivity was found for *BG-SA* and *BG-SL* scaffolds. In the case of *BG-SA* the average diffusivity is only half the effective diffusivity of BG-PU and for *BG-SL* only a third of this value is obtained. However, the mechanical strength of *BG-SA* and *BG-SL* scaffolds exceeds that of *BG-PU* scaffolds by a factor of at least 40 and the optimum scaffold geometry depends on the combination of strength requirements, diffusivity and biological compatibility. Thus the methodology introduced in this study is relevant to select bone tissue engineering scaffolds incorporating quantification of diffusivity as a relevant parameter to consider.

**Acknowledgments** This research was supported under the Australian Research Council Discovery Projects funding scheme (Project Number DP130101377). In addition, this research was carried out in the framework of the EU ITN FP-7 Project "GlaCERCo". The authors would like to acknowledge its financial support.

## References

1. Gómez-Barrena E, Rosset P, Lozano D, Stanovici J, Ermthaller C, Gerbhard F. Bone fracture healing: cell therapy in delayed unions and nonunions. Bone. 2015;70:93–101.
2. Stevens MM. Biomaterials for bone tissue engineering. Mater Today. 2008;11:18–25.
3. Mulvana H. New materials and technologies for healthcare. In: Hench LL, Jones JR, Fenn MB, editors. London: Imperial College Press; 2011, p. 520, ISBN: 978-1-84816-558-8; Ultrasound in medicine & biology. vol. 40; 2//2014. p. 457.
4. Hutmacher DW. Scaffolds in tissue engineering bone and cartilage. Biomaterials. 2000;21(24):2529–43.
5. Gerhardt L-C, Boccaccini AR. Bioactive glass and glass-ceramic scaffolds for bone tissue engineering. Materials. 2010;3:3867–910.
6. Polak JM, Hench LL, Kemp P. Future strategies for tissue and organ replacement. Singapore: World Scientific Publishing Company; 2002.
7. Hench LL. The story of bioglass. J Mater Sci Mater Med. 2006;2006(17):967–78.
8. Jones JR. Review of bioactive glass: from Hench to hybrids. Acta Biomater. 2013;9:4457–86.
9. Gorustovich AA, Roether JA, Boccaccini AR. Effect of bioactive glasses on angiogenesis: a review of in vitro and in vivo evidences. Tissue Eng Part B. 2009;16(2):199–207.
10. Chen QZ, Thompson ID, Boccaccini AR. 45S4 Bioglass-derived glass ceramic scaffolds for bone tissue engineering. Biomaterials. 2006;27:2414–25.
11. Cunningham E, Dunne N, Clarke S, Choi SY, Walker G, Wilcox R, et al. Comparative characterization of 3-D hydroxyapatite scaffolds developed via replication of synthetic polymer foams and natural marine sponges. J Tissue Sci Eng. 2011. doi:10.4172/2157-7552.S1-001.
12. Karande TS. Effect of scaffold architecture on diffusion of oxygen in tissue engineering constructs. PhD, The University of Texas at Austin, 2007.
13. Kang TY, Kang HW, Hwang CM, Leel SJ, Park J, Yoo JJ, et al. The realistic prediction of oxygen transport in a tissue-engineered scaffold by introducing time-varying effective diffusion coefficients. Acta Biomater. 2011;7:3345–53.
14. Fiedler T, Belova IV, Murch GE, Jones JR, Roether JA, Boccaccini AR. A comparative study of oxygen diffusion in tissue engineering scaffolds. J Mater Sci Mater Med. 2014;25:2573–8.
15. Pronzato R, Manconi R. Mediterranean commercial sponges: over 5000 years of natural history and cultural heritage. Mar Ecol. 2008;29:146–66.

16. Yang S, Leong KF, Du Z, Chua CK. The design of scaffolds for use in tissue engineering—traditional factors. Tissue Eng. 2001;7:679–89.
17. Mastrogiacomo M, Scaglione S, Martinetti R, Dolcini L, Beltrame F, Cancedda R, et al. Role of scaffold internal structure on in vivo bone formation in macroporous calcium phosphate bioceramics. Biomaterials. 2006;27:3230–7.
18. Boccardi E, Philippart A, Juhasz-Bortuzzo JA, Novajra G, Vitale-Brovarone C, Boccaccini AR. Characterisation of Bioglass®-based foams developed via replication of natural marine sponges. Adv. Appl Ceram. 2015 (**accepted for publication**).
19. Hench L, Wilson J. Surface-active biomaterials. Science. 1984;226:630–6.
20. Kokubo T, Takadama H. How useful is SBF in predicting in vivo bone bioactivity? Biomaterials. 2006;27:2907–15.
21. Fiedler T, Belova IV, Rawson A, Murch GE. Optimized lattice Monte Carlo for thermal analysis of composite. Comput Mater Sci. 2014;95:207–12.
22. Belova IV, Murch GE, Fiedler T, Öchsner A. Lattice-based walks and the Monte Carlo method for addressing mass, thermal and elasticity problems. Defect Diffus Forum. 2008;283–286:3–23.
23. Fiedler T, Belova IV, Murch GE. Theoretical and lattice Monte Carlo analyses on thermal conduction in cellular metals. Comput Mater Sci. 2010;50:503–9.
24. Fiedler T, Belova IV, Öchsner A, Murch GE. A review on thermal lattice Monte Carlo analysis. In: Delgado JM, editor. Current trends in chemical engineering. Houston: Studium Press LCC; 2010. p. 105–30.
25. Solorzano E, Reglero JA, Rodríguez-Perez MA, Lehmhus D, Wichmann M, De Saja JA. An experimental study on the thermal conductivity of aluminium foams by using the transient plane source method. Int J Heat Mass Transf. 2008;51:6259–67.
26. Maxwell JC. A treatise on elasticity and magnetism. Oxford: Clarendon Press; 1892.
27. Dulnev GN. Heat transfer through solid disperse systems. J Eng Phys. 1965;9:275–9.
28. Doube M, Kłosowski MM, Arganda-Carreras I, Cordeliéres F, Dougherty RP, Jackson J, et al. BoneJ: free and extensible bone image analysis in ImageJ. Bone. 2010;47:1076–9.